American Mineralogist, Volume 74, pages 764–773, 1989

Effects of oxidation-dehydrogenation in tschermakitic hornblende

Michael W. Phillips
Department of Geology, The University of Toledo, Toledo, Ohio 43606, U.S.A.
James E. Draheim
Department of Chemistry, Adrian College, Adrian, Michigan 49221, U.S.A.
Robert K. Popp, Celia A. Clowe*
Department of Geology, Texas A&M University, College Station, Texas 77843, U.S.A.
A. Alan Pinkerton
Department of Chemistry, The University of Toledo, Toledo, Ohio 43606, U.S.A.

Abstract

Crystal-structure refinements and diffuse-reflectance-infrared Fourier-transform spectra in the region of the fundamental hydroxyl stretch frequencies have been used to examine subtle structural changes that result from partial oxidation-dehydrogenation in a tschermakitic hornblende. The samples examined were H-1, the natural, untreated material (Fe^{3+} = 0.389 pfu); H-11, material hydrothermally annealed at 650 °C and 1 kbar for 4 d at the magnetite-hematite oxygen buffer (Fe^{3+} = 0.565 pfu); and H-3, material air-heated at 700 °C and 1 atm for 30 min (Fe^{3+} = 0.869 pfu).

On the basis of the increase in Fe^{3+} contents, the loss of H accompanying oxidation was calculated to be 0.18 and 0.48 H per formula unit for H-11 and H-3, respectively, relative to H-1. Direct estimates of H contents by unconstrained site refinement indicated respective losses of 0.22 and 0.66 H per formula unit.

Bond-length data indicate that the concentration of trivalent cations increases at M(1) and M(3), but decreases at M(2) as oxidation proceeds. However, the decrease in M–O(3) bond lengths in H-11 and H-3 is even greater than would be expected based on cation content alone.

There is also evidence for interaction between O(3) and the A-site cation in the oxidized structures. Shortening of the A(*m*)–O(3) distances in H-11 and H-3 appears to be related to the extent of oxidation, and there is an increase in the occupancy at A(*m*) in H-3. Furthermore, the decrease in the width of the infrared absorption region with increased oxidation suggests that dehydrogenation preferentially occurs at O(3) sites in the vicinity of occupied, rather than vacant, A sites.

Introduction

During the past century there have been a number of studies concerning the oxidation behavior of Fe-bearing amphiboles. The reader is referred to Barnes (1930) for a review of the early work and to Hawthorne (1983) for a review of recent investigations.

Results from the extensive heating experiments of Barnes (1930) suggested that in hornblendes and actinolites, oxidation proceeds by a dehydrogenation reaction of the type

$$Fe^{2+} + OH^- = Fe^{3+} + O^{2-} + \tfrac{1}{2}H_2$$

This reaction has also been found to be the initial oxidation mechanism in alkali amphiboles (e.g., see Ernst and Wai, 1970).

Most studies performed to date have relied on spectroscopic techniques for structural characterization of heat-treated specimens. Although these techniques have proved useful in monitoring dehydrogenation and even in detecting cation migration (e.g., see Ernst and Wai, 1970), they do not provide the detailed structural information available from crystal-structure refinements performed before and after heating experiments. However, prior to this investigation, the only such study reported was by Ungaretti (1980), who published preliminary crystal-structure refinement results for a metamorphic riebeckite sample before and after it was heated in air at 650 °C for 4 d.

The purpose of this study is to investigate the subtle structural changes that accompany oxidation-dehydrogenation in a natural tschermakitic hornblende. Crystal-structure refinements and infrared spectra are reported for samples that were untreated (H-1), hydrothermally annealed at 650 °C and 1 kbar for 4 d at the magnetite-

* Present address: Department of Geological Sciences, Virginia Polytechnic Institute and State University, Blacksburg, Virginia 24061, U.S.A.

0003–004X/89/0708–0764$02.00

TABLE 1. Chemical formula and unit cell parameter data

	H-1	H-11	H-3
Conditions	natural	650 ° C, 1 kbar, 4 d, MH	700 ° C, 1 atm, 30 min, air
$R = Fe^{3+}/(Fe^{2+} + Fe^{3+})$	0.21	0.30	0.47
Fe^{3+} (pfu)*	0.412	0.588	0.921
Fe^{3+} (pfu)	0.389	0.565	0.869
$X = OH$ (pfu)	1.84	1.66	1.36
Calculated density	3.244 g/cm³	3.255 g/cm³	3.268 g/cm³
	Unit-cell dimensions**		
a (Å)	9.813(2)	9.803(2)	9.786(3)
b (Å)	18.055(3)	18.046(4)	18.024(5)
c (Å)	5.321(1)	5.313(1)	5.306(2)
β (°)	104.97(2)	105.05(2)	105.09(3)
V (Å³)	910.8(6)	907.7(6)	903.6(10)
	General formula (all three samples)		
	$K_{0.09}Na_{0.41}(Ca_{1.83}Mn_{0.04}Fe_{1.96}Mg_{2.17}Al_{0.86}Ti_{0.07})(Al_{1.57}Si_{6.43})O_{22}(F_{0.06}OH_xO^{2-}_{1.94-x})$		

* These values are based on the total Fe per formula unit (1.96) as determined by microprobe analysis. The values given in the row below are based on the total Fe per formula unit as determined by site refinement and were used to estimate the OH contents.

** Estimated standard deviations are given in parentheses and refer to the last decimal place.

hematite (MH) oxygen buffer (H-11), and heated in air at 700 °C and 1 atm for 30 min (H-3). The details of the heating experiments are given by Clowe et al. (1988).

Experimental procedures

Sample description

The natural sample is from a kyanite-staurolite–grade amphibolite described by Spear (1982, sample 73-31B). Clowe et al. (1988) performed extensive heating experiments on the sample under both oxidizing and reducing conditions and reported the ferric-ferrous ratios, $R = Fe^{3+}/(Fe^{2+} + Fe^{3+})$, on all run products as determined by the method of Fritz and Popp (1985). Clowe et al. (1988) reported a value of $R = 0.21$ for the natural material, which only dropped to $R = 0.15$ after being annealed for both 4 and 8 d at 650 °C and 1 kbar under the reducing conditions provided by the graphite-methane buffer. This suggests that the majority of the Fe^{3+} present ($R = 0.15$) is a trivalent proxy for octahedral Al, whereas only a small amount ($R = 0.06$) is present because of oxy-amphibole component (Clowe et al., 1988).

The electron-microprobe analysis of the untreated material reported by Clowe et al. (1988, Table 1) was recalculated to 23.06 oxygens based on the assumed oxy-amphibole content and was used for all three cyrstals (H-1, H-11, H-3) examined. The Fe^{3+} content per formula unit for H-1, H-11, and H-3 was calculated from the respective R determinations of Clowe et al. (1988). The H content per formula unit was then calculated on the basis of the dehydrogenation reaction and these values for Fe^{3+} (excluding the 0.29 Fe^{3+} per formula unit that is considered to act as an Al proxy). These data, along with unit-cell parameters determined by least-squares refinement of sets of 25 diffractometer-centered reflections, are given in Table 1.

X-ray data collection and refinement

Intensities of all reflections in a hemisphere ($k \geq 0$) of radius $\sin\theta/\lambda = 0.81$ were measured by an automated ENRAF-NONIUS CAD4 diffractometer using graphite-monochromatized Mo$K\alpha$ radiation ($\lambda = 0.71073$ Å). An attenuator was automatically inserted for intense reflections. Background counts were determined by scanning 25% above and below the peak scan range. Data collection and refinement parameters are given in Table 2.

Data were corrected for background and Lorentz-polarization effects. Absorption corrections were intitially made on the basis of a series of ψ-scans (North et al.,

TABLE 2. Data collection and refinement parameters

	H-1	H-11	H-3
Conditions	natural	650 ° C, 1 kbar, 4 d, MH	700 ° C, 1 atm, 30 min, air
Space group	$C2/m$	$C2/m$	$C2/m$
Crystal size (mm)	0.15 × 0.05 × 0.04	0.17 × 0.06 × 0.03	0.12 × 0.05 × 0.05
Max. $\sin\theta/\lambda$	0.8058	0.8062	0.8062
Scan speed (°/min)	1–7	1–7	1–7
Scan width	0.8 + 0.34 tan θ	0.8 + 0.34 tan θ	0.9 + 0.34 tan θ
Total reflections (excluding stds.)	4114	4095	4081
Unique reflections	2064	2055	2048
Averaging agreement (on F) for accepted reflections	2.0%	2.2%	2.7%
Accepted reflections	1317	1265	1190
μ(cm⁻¹)	29.14	29.24	29.37
Extinction coefficient	8.8(3) × 10^{-7}	6.4(3) × 10^{-7}	2.3(5) × 10^{-7}
Final R	2.19%	2.24%	3.54%
Final R_w	2.32%	2.37%	3.66%

1968) and subsequently improved using the empirical method of Walker and Stuart (1983). Reflections with $I < 3\sigma(I)$ (as determined by counting statistics) were considered unobserved and marked for rejection. Equivalent reflections were averaged and reflections of the type $|I - I_{avg}| > 5\sigma(I)$ were also marked for rejection.

Scattering factors for neutral atoms and correction factors for anomalous dispersion effects (Ibers and Hamilton, 1964) were taken from the *International Tables for X-ray Crystallography* (1974). An isotropic extinction coefficient (Zachariasen, 1963, 1967) was included as a variable in all refinements. All calculations were performed on a VAX11/750 computer using the manufacturer-supplied SDP/VAX software package.

On the basis of the chemical formula given in Table 1, tetrahedral Al was assigned to T(1), octahedral Al and Ti were assigned to M(2), and Ca was assigned to M(4). The small amounts of Mn (0.04 pfu) and F (0.06 pfu) were treated as Fe and O, respectively, for purposes of refinement because of similarities of their respective scattering powers. The A cation was assumed to be Na (the 0.09 K was neglected) and was initially assumed to reside at the A(2/*m*) site (see Hawthorne, 1983, p. 254). The Fe-Mg cations were initially assumed to be randomly distributed among M(1) and M(3) and the unassigned portion of M(2).

The initial refinements—employing isotropic temperature factors, unit weights, and positional parameters taken from a compositionally similar amphibole (Hawthorne, 1983, App. B2)—converged rapidly. Site refinements were then performed on the M sites and assumed that only Fe and Mg vary; the total site occupancy of each individual M site was constrained to 1.0. These refinements were repeated with initial occupancies first assumed to be predominantly Fe and then predominantly Mg. Regardless of the initial Fe-Mg occupancies, all refinements converged to the same values. In subsequent refinements, the occupancies of Na at both M(4) and A(2/*m*) were allowed to refine without constraints.

After location of the H positions by difference-Fourier methods, all atoms except H were assumed to vibrate anisotropically in subsequent refinements. In the final refinement, all positional parameters, anisotropic temperature factors (except for H where B was fixed at 0.5), the constrained Fe-Mg occupancies of M(1), M(2), M(3), and the unconstrained multiplicities of H and Na at A(2/*m*) were allowed to vary simultaneously. This refinement was used to obtain the final atomic and thermal parameters, interatomic distances and angles, and site-occupancy data reported in Tables 3, 4, and 5, respectively. A complete list of observed and calculated structure factors are given in Tables 6, 7, and 8 for the respective structures.[1] Subsequent refinements that examined M(4′) and split-atom models for the A site are discussed in a later section.

[1] A copy of Tables 6, 7, and 8 may be ordered as Document AM-89-409 from the Business Office, Mineralogical Society of America, 1625 I Street, N.W., Suite 414, Washington, D.C. 20006, U.S.A. Please remit $5.00 in advance for the microfiche.

It appears that H-3 may have experienced some structural damage during the rapid oxidation-dehydrogenation produced by air-heating. The reflections for H-3 were broader than those for H-1 and H-11 in both powder-diffraction tracings and peak profiles measured on the CAD4. This broadening may account for the higher R values and the larger esd's obtained for this data set. It may also account for the larger variations observed for $w\Delta F^2$ in the H-3 data set.

Inspection of data from the final refinements indicated that unit weights satisfactorily minimized the variation of $w\Delta F^2$ as a function of the magnitude of F_o, (see Cruickshank, 1965) for H-1 and H-11, but not for H-3. Both the most intense (upper 5%) and least intense (lower 10%) structure factors in the H-3 data set had average values of $w\Delta F^2$ that were 3–6 times larger than for the majority of the data set. Even so, it was decided to retain unit weights for H-3 in order to treat all three data sets in a consistent manner.

Infrared spectra

The mid-infrared spectra of the samples were measured using a Nicolet 60SX FTIR spectrometer equipped with a specially designed DRIFT accessory. The 60SX FTIR spectrometer has a 36-megabyte hard disk and was operated using the Nicolet menu-driven software, version 2.3. A DTGS detector was used with KBr windows. The spectra were measured to a resolution of 4 cm^{-1} using the standard data collection parameters of the 2.3 software package. The number of repetitions was set at 200 scans for both the sample and background files. The samples were carefully ground into fresh dry KBr to form a uniform sample material prior to packing into the DRIFT unit sample holder; KBr alone was used for the background file. The spectra were corrected for both water and carbon dioxide interference using water and carbon dioxide background spectra collected previously the same day. No additional baseline and/or spectral corrections were performed. The first-derivative spectra were calculated from the collected spectra using the DRI software option.

Results

X-ray results

The M(1), M(2), M(3) sites. Examination of the site-refinement results for Mg-Fe (Table 5) indicates that appreciable octahedral-cation migration accompanies oxidation, even in H-3, which was air-heated for only 30 min. Using Mössbauer spectroscopy, Ernst and Wai (1970) were able to detect cation migration in alkali amphiboles heat-treated under similar conditions, but only for longer-duration experiments. The total Fe content of M(2) increased with increasing oxidation whereas total Fe content of M(3) decreased. The total Fe content of M(1) is the same for H-1 and H-11, but larger in H-3.

Distinguishing Fe^{2+} from Fe^{3+} in a given site from structure-refinement data alone presents a difficult problem, and the degree of difficulty rises dramatically as the

TABLE 3. Final atomic parameters

Atom	Structure	x	y	z	U_{11}	U_{22}	U_{33}	U_{12}	U_{13}	U_{23}	B_{eq}
T(1)	H-1	0.28020(5)	0.08606(3)	0.30109(10)	58(2)	63(2)	63(2)	−11(2)	9(1)	−2(2)	0.494(8)
	H-11	0.28110(6)	0.08682(3)	0.30119(11)	69(2)	68(2)	71(2)	−7(2)	12(2)	−3(2)	0.557(8)
	H-3	0.28216(10)	0.08563(5)	0.30101(18)	74(3)	66(3)	68(3)	−9(3)	6(3)	2(3)	0.57(1)
T(2)	H-1	0.29168(5)	0.17334(3)	0.81442(10)	61(2)	70(2)	66(2)	−1(2)	14(1)	7(2)	0.520(7)
	H-11	0.29154(6)	0.17306(3)	0.81322(11)	71(2)	76(2)	75(2)	1(2)	17(2)	7(2)	0.587(8)
	H-3	0.29167(10)	0.17291(5)	0.81243(18)	73(3)	65(3)	77(3)	1(3)	19(2)	11(3)	0.57(1)
M(1)	H-1	0.0	0.08972(3)	0.5	83(2)	66(2)	57(2)	0	20(2)	0	0.538(8)
	H-11	0.0	0.08869(4)	0.5	93(2)	89(2)	67(2)	0	23(2)	0	0.652(9)
	H-3	0.0	0.08686(6)	0.5	95(4)	118(4)	79(3)	0	34(2)	0	0.75(2)
M(2)	H-1	0.0	0.17782(4)	0.0	56(2)	61(2)	63(3)	0	13(2)	0	0.48(1)
	H-11	0.0	0.17764(4)	0.0	72(2)	65(2)	72(2)	0	16(2)	0	0.56(1)
	H-3	0.0	0.17738(6)	0.0	73(4)	66(4)	81(4)	0	17(3)	0	0.58(2)
M(3)	H-1	0.0	0.0	0.0	79(3)	56(3)	58(2)	0	13(2)	0	0.52(1)
	H-11	0.0	0.0	0.0	93(3)	64(3)	72(3)	0	12(2)	0	0.62(1)
	H-3	0.0	0.0	0.0	96(5)	41(5)	75(5)	0	14(4)	0	0.57(2)
M(4)	H-1	0.0	0.28038(3)	0.5	104(2)	97(2)	104(2)	0	52(2)	0	0.766(8)
	H-11	0.0	0.27999(3)	0.5	117(2)	97(2)	118(2)	0	55(2)	0	0.840(9)
	H-3	0.0	0.27950(6)	0.5	112(3)	93(3)	106(3)	0	55(3)	0	0.78(1)
O(1)	H-1	0.1057(1)	0.0920(1)	0.2116(3)	79(5)	168(6)	96(5)	−26(5)	27(4)	−17(5)	0.89(2)
	H-11	0.1063(2)	0.0906(1)	0.2132(3)	93(5)	165(6)	107(5)	−20(5)	30(4)	−10(5)	0.96(2)
	H-3	0.1073(3)	0.0896(2)	0.2141(5)	100(9)	180(10)	101(9)	−27(4)	20(7)	−12(9)	1.00(4)
O(2)	H-1	0.1195(1)	0.1753(1)	0.7385(3)	70(5)	99(5)	112(5)	2(5)	11(4)	9(5)	0.76(2)
	H-11	0.1192(2)	0.1743(1)	0.7356(3)	78(5)	133(6)	111(6)	6(5)	11(4)	16(5)	0.87(2)
	H-3	0.1188(3)	0.1734(1)	0.7333(5)	65(8)	122(9)	116(9)	2(8)	−5(7)	14(8)	0.84(4)
O(3)	H-1	0.1108(2)	0.0	0.7115(4)	71(7)	114(8)	125(8)	0	8(6)	0	0.84(3)
	H-11	0.1102(2)	0.0	0.7136(5)	85(8)	132(8)	164(9)	0	14(7)	0	1.03(4)
	H-3	0.1093(4)	0.0	0.7142(7)	110(10)	140(10)	110(10)	0	−3(10)	0	1.00(6)
O(4)	H-1	0.3696(2)	0.2505(1)	0.7943(3)	132(5)	86(5)	123(5)	−18(5)	51(4)	−8(5)	0.87(2)
	H-11	0.3686(2)	0.2505(1)	0.7930(3)	143(6)	98(5)	131(6)	−13(5)	50(5)	−4(5)	0.96(2)
	H-3	0.3670(3)	0.2506(2)	0.7932(5)	146(9)	94(9)	160(10)	−15(9)	68(8)	−10(9)	1.00(4)
O(5)	H-1	0.3506(2)	0.1394(1)	0.1093(3)	84(5)	146(6)	100(5)	−1(5)	8(4)	51(5)	0.89(2)
	H-11	0.3504(2)	0.1395(1)	0.1089(3)	105(5)	152(6)	123(6)	2(5)	14(5)	47(5)	1.02(2)
	H-3	0.3501(3)	0.1394(2)	0.1066(5)	87(9)	160(10)	144(9)	−2(9)	18(7)	58(9)	1.06(4)
O(6)	H-1	0.3421(2)	0.1198(1)	0.6020(2)	92(5)	136(6)	130(6)	2(5)	18(4)	−35(5)	0.96(2)
	H-11	0.3430(2)	0.1195(1)	0.6021(3)	104(6)	137(6)	136(6)	−2(5)	19(5)	−36(5)	1.01(2)
	H-3	0.3441(3)	0.1195(1)	0.6019(5)	102(10)	140(10)	123(9)	14(9)	20(8)	−42(9)	1.03(4)
O(7)	H-1	0.3333(2)	0.0	0.2860(5)	154(9)	140(8)	179(9)	0	30(8)	0	1.26(4)
	H-11	0.3353(3)	0.0	0.2861(5)	154(9)	134(9)	200(10)	0	30(8)	0	1.29(4)
	H-3	0.3371(4)	0.0	0.2870(8)	170(20)	160(20)	190(20)	0	30(10)	0	1.40(7)
A(2/*m*)	H-1	0.0	0.5	0.0	440(30)	1900(100)	770(40)	0	520(20)	0	7.8(3)
	H-11	0.0	0.5	0.0	1570(40)	1070(80)	1910(40)	0	1660(20)	0	10.2(2)
	H-3	0.0	0.5	0.0	2760(70)	900(100)	3250(80)	0	2850(40)	0	15.0(4)
H	H-1	0.325(5)	0.5	0.245(10)	For hydrogen in H-1, H-11, H-3, the isotropic temperature factors were arbitrarily fixed at $B = 0.5$						
	H-11	0.319(6)	0.5	0.268(11)							
	H-3	0.291(13)	0.5	0.263(23)							

Note: The thermal parameters are of the form $\exp[-2\pi^2(U_{11}h^2a^{*2} + U_{22}k^2b^{*2} + U_{33}l^2c^{*2} + 2U_{12}hka^*b^* + 2U_{13}hla^*c^* + 2U_{23}klb^*c^*)]$ and are multiplied by 10^4. Estimated standard deviations are given in parentheses and refer to the least significant digit.

number of types of different cations in the octahedral strip increases. Site refinement cannot distinguish the two, and the size difference between Fe^{2+} and Fe^{3+} octahedra is only about 5% as compared to about a 9% difference for Al and Si tetrahedra. Hawthorne (1981a, 1983) has established a set of ideal mean M–O bond lengths for M(1), M(2), and M(3) sites completely occupied by different single cations for structures in which O(3) = OH. However, Hawthorne (1981a, 1983) cautioned that the exact size of M(1) and M(3) depends in part on the identity of O(3), and he also pointed out that the size of M(3) may be slightly influenced by the average cation size in M(2).

With these problems in mind, ideal ⟨M–O⟩ bond lengths were calculated for H-1, H-11, and H-3 by using Hawthorne's ideal values in conjunction with the site occupancies given in Table 5, treating all Fe present as Fe^{2+}. The parameter $\Delta\langle M\text{–}O\rangle = \langle M\text{–}O\rangle_{calc} - \langle M\text{–}O\rangle_{obs}$ was then calculated for all sites using the observed ⟨M–O⟩ bond lengths. Because Fe^{2+} is slightly larger than Fe^{3+}, a large positive value of $\Delta\langle M\text{–}O\rangle$ indicates the presence of Fe^{3+}. Plots of $\Delta\langle M\text{–}O\rangle$ against the total Fe^{3+} per formula unit

TABLE 4. Selected interatomic distances (Å) and angles (°)

	H-1	H-11	H-3		H-1	H-11	H-3
T(1)–O(1)	1.658(1)	1.657(1)	1.654(2)	M(1)–O(1) ×2	2.063(1)	2.058(1)	2.058(2)
–O(5)	1.677(1)	1.675(2)	1.674(2)	–O(2) ×2	2.146(1)	2.134(1)	2.137(2)
–O(6)	1.674(1)	1.670(2)	1.669(2)	–O(3) ×2	2.107(1)	2.093(1)	2.062(2)
–O(7)	1.647(1)	1.646(1)	1.642(1)	mean	2.105	2.095	2.086
mean	1.664	1.662	1.660				
				M(2)–O(1) ×2	2.035(1)	2.056(2)	2.068(2)
O(1)–T(1)–O(5)	110.22(7)	110.58(7)	110.56(10)	–O(2) ×2	2.039(1)	2.048(1)	2.053(2)
–O(6)	110.13(7)	110.08(7)	110.02(10)	–O(4) ×2	1.945(1)	1.953(1)	1.959(2)
–O(7)	111.29(9)	110.98(9)	110.78(12)	mean	2.006	2.019	2.027
O(5)–T(1)–O(6)	105.57(7)	105.61(8)	105.91(10)				
–O(7)	109.06(9)	109.13(9)	109.23(13)	M(3)–O(1) ×4	2.121(1)	2.104(1)	2.093(2)
O(6)–T(1)–O(7)	110.41(9)	110.32(9)	110.22(13)	–O(3) ×2	2.098(2)	2.082(2)	2.071(3)
mean	109.45	109.45	109.45	mean	2.113	2.097	2.086
T(2)–O(2)	1.633(1)	1.632(1)	1.634(2)	M(4)–O(2) ×2	2.411(1)	2.411(1)	2.407(2)
–O(4)	1.607(1)	1.606(1)	1.599(2)	–O(4) ×2	2.331(1)	2.330(1)	2.337(2)
–O(5)	1.644(1)	1.642(2)	1.632(2)	–O(5) ×2	2.645(1)	2.645(1)	2.655(2)
–O(6)	1.657(1)	1.656(1)	1.654(2)	–O(6) ×2	2.525(1)	2.527(1)	2.523(2)
mean	1.635	1.634	1.630	mean	2.478	2.478	2.481
O(2)–T(2)–O(4)	116.38(7)	116.46(7)	116.32(10)	A(2/*m*)–O(5) ×4	3.043(1)	3.044(1)	3.036(2)
–O(5)	109.32(7)	109.28(8)	109.21(10)	A(2/*m*)–O(6) ×4	3.142(1)	3.130(1)	3.123(2)
–O(6)	108.45(7)	108.31(7)	108.16(10)	A(2/*m*)–O(7) ×2	2.506(2)	2.489(2)	2.475(3)
O(4)–T(2)–O(5)	109.33(7)	109.29(7)	109.43(10)	A(2/*m*)–O(7) ×2	3.728(2)	3.717(2)	3.703(3)
–O(6)	103.25(7)	103.39(7)	103.74(10)				
O(5)–T(2)–O(6)	109.86(7)	109.86(8)	109.74(10)	T(1)–O(5)–T(2)	134.14(8)	134.38(4)	135.01(12)
mean	109.43	109.43	109.43	T(1)–O(6)–T(2)	140.01(9)	139.64(9)	139.47(12)
				T(1)–O(7)–T(1)	141.20(14)	140.43(15)	140.02(20)
H–O(3)	0.61(5)	0.68(6)	0.95(9)	O(5)–O(6)–O(5)	164.50(8)	164.50(8)	164.41(10)
				O(7)–O(7)–O(7)	65.62(7)	65.31(8)	65.09(10)

Note: Estimated standard deviations are given in parentheses and refer to the least significant digit.

as determined from the R ratios of Clowe et al. (1988) are given in Figure 1 for M(1), M(2), and M(3).

As part of a study of bond-strength variations in oxidized amphiboles, Phillips et al. (1988a) were able to obtain Fe^{3+}-Fe^{2+} site occupancies in these structures using the ideal bond lengths. As they noted, these assignments are highly speculative because of the number of assumptions required. Phillips et al. (1988a) also pointed out that errors in assigning Fe^{3+}-Fe^{2+} (or Al-Mg) have little or no impact on bond strengths calculated with the Brown and Wu (1976) parameters. Nevertheless, in the absence of more direct evidence, such as Mössbauer spectra, further speculation as to the exact distribution of Fe^{3+} in these structures is not warranted. However, comparison of the $\Delta\langle M\text{–}O\rangle$ parameters can provide general information about changes in the distribution of the small trivalent cations.

As expected, the grand mean octahedral bond lengths

TABLE 5. Site occupancies

	H-1		H-11		H-3	
	Al	Si	Al	Si	Al	Si
T(1)	0.39	0.61	0.39	0.61	0.39	0.61
T(1)*	0.35	0.65	0.34	0.66	0.32	0.68
T(2)	0.0	1.0	0.0	1.0	0.0	1.0
T(2)*	0.02	0.98	0.01	0.99	−0.02	1.0
	Fe	Mg	Fe	Mg	Fe	Mg
M(1)	0.415(2)	0.585	0.413(2)	0.587	0.443(4)	0.557
M(2)**	0.214(2)	0.321	0.284(2)	0.251	0.256(4)	0.279
M(3)	0.588(3)	0.412	0.490(3)	0.510	0.454(6)	0.546
	Ca	Na	Ca	Na	Ca	Na
M(4)	0.915	0.099(4)	0.915	0.097(4)	0.915	0.073(6)
A(2/*m*)	0.43(1)Na		0.47(1)Na		0.56(2)Na	
H	0.92		0.83		0.68	
H	1.00(10)		0.89(10)		0.67(16)	

Note: The Fe-Mg, Na, and H values with estimated standard deviations in parentheses were determined by site refinement as described in the text. All other values not specifically footnoted were assigned on the basis of the chemical analyses in Table 1.

* These values were calculated from mean bond-length data using the equations of Hawthorne and Grundy (1977).

** All M(2) sites also contained 0.430 Al and 0.035 Ti assigned on the basis of the chemical analysis.

[= (2⟨M(1)–O⟩ + 2⟨M(2)–O⟩ + ⟨M(3)–O⟩)/5] decrease slightly from H-1 (2.067) to H-11 (2.065) to H-3 (2.062 Å), reflecting the increase in smaller Fe^{3+} cation content resulting from oxidation. The amounts of smaller cations occupying M(1) and M(3) also increase with oxidation, as demonstrated by the positive slopes of the Δ⟨M–O⟩ parameters in Figures 1A and 1C, respectively. However, the trend is opposite for M(2) (Fig. 1B), which means that smaller cations (such as Fe^{3+} and Al) are replaced by larger cations (such as Fe^{2+} and Mg) as oxidation proceeds. In order to perform site refinement on Fe-Mg, all octahedral Al was constrained to M(2) in each structure. However, because Al and Mg have similar scattering powers, the lower Mg contents in M(2) for H-11 and H-3 (Table 5) may actually represent a loss of Al, rather than Mg, from M(2). In any event, it is clear that as oxidation proceeds, the Fe^{3+} cations produced by oxidation, as well as some trivalent cations initially in M(2) (Fe^{3+} and perhaps Al), preferentially order at M(1) and M(3).

The M(4) site. It was assumed that in addition to the 0.915 Ca present as determined by electron-microprobe analysis (Clowe et al., 1988), M(4) was also occupied by Na in all three structures. The occupancy of Na in M(4) was allowed to refine unconstrained, and the resulting occupancies are given in Table 5.

In H-1 and H-11 the total site occupancy slightly exceeds 1.0 (1.014 and 1.012, respectively). This excess may be due to small errors in the Ca analysis. In H-3, the Na occupancy determined by site refinement is 0.073(6) as compared to the values of 0.099(4) and 0.097(4) for H-1 and H-11, respectively. It appears likely that this decrease represents a migration of Na from M(4) to the A site. Ungaretti (1980) found that in an air-heated riebeckite, there was extensive occupancy of the previously vacant A site by Na derived from M(4), resulting in vacancies at M(4).

The H site. The H position in all three structures was readily located by difference-Fourier methods. A full matrix refinement was attempted including the multiplicity, positional coordinates (x, z) and isotropic temperature factor (B) of H as variables with the parameter shifts dampened to 0.5 to assure convergence rather than oscillation about a minimum. These refinements yielded values of B = 2.27 (1.09), 0.53 (1.17), and 0.14 (2.13) and occupancies of 1.09 (0.10), 0.89 (0.10), and 0.74 (0.16) for H-1, H-11, and H-3, respectively. Because of the large errors in B and because of high correlations between temperature factors and occupancies, the isotropic temperature factors for H in all three structures were arbitrarily fixed at 0.5, the value obtained by Papike et al. (1969) for H in tremolite. Subsequent refinements with B fixed at 0.5 yielded H occupancies that are in good agreement with those estimated from the Fe^{3+} contents (see Table 5). A plot of these occupancies against the total Fe^{3+} per formula unit due only to oxy-amphibole component, as determined from the analyses of Clowe et al. (1988), is shown in Figure 2. Similar attempts to refine H occupancies in a suite of magnesio-hornblende structures were not as successful (Phillips et al., unpublished data). Therefore, it is not clear whether the results shown in Figure 2 are fortuitous or whether the high F content (0.33 pfu) of the magnesio-hornblendes precluded refinement.

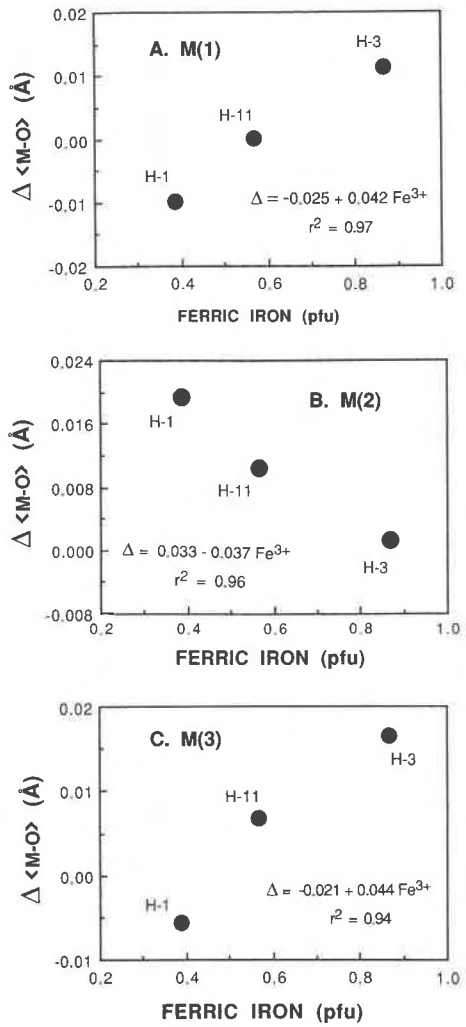

Fig. 1. Variation of Δ⟨M–O⟩ (= $\langle M\text{–}O\rangle_{calc} - \langle M\text{–}O\rangle_{obs}$) with total Fe^{3+} per formula unit. (**A**) The M(1) site, (**B**) the M(2) site, (**C**) the M(3) site. $\langle M\text{–}O\rangle_{calc}$ was calculated treating all Fe as Fe^{2+}. Therefore the positive slopes in A and C indicate increases in small trivalent cation contents at M(1) and M(3) as oxidation proceeds, whereas the negative slope in B represents a decrease at M(2).

The A site. The occupancies of the A site, as determined by unconstrained refinement of occupancies (Table 5), indicate an apparent increase in Na content per formula unit with increasing oxidation from 0.43(1) in H-1 to 0.47(1) in H-11 to 0.56(2) in H-3. Some of the increase in H-3 is probably due to a slight migration of Na from M(4) to A as was observed on a larger scale in oxidized riebeckite (Ungaretti, 1980). However, some of the increase may also be attributed to the progressive increase in the apparent size of the average A site that

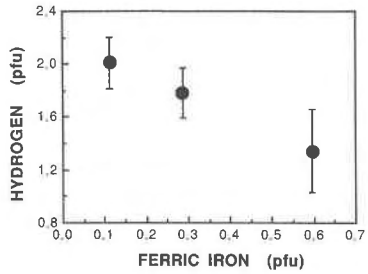

Fig. 2. Variation of H per formula unit as determined by site refinement with Fe^{3+} per formula unit due only to oxy-amphibole component. Error bars for H represent one estimated standard deviation.

accompanies oxidation. This can be gauged by the increase of the equivalent isotropic temperature factors for the A site from 7.8(3) for H-1 to 10.2(2) for H-11 to 15.0(4) for H-3.

Difference-Fourier maps through various sections of the A site were computed with the Na atom omitted from the structure-factor calculations. The *y-z* section, which is coincident with the mirror plane, showed a marked anisotropy with the elongate axis pointed in the general direction of O(3). The extent of the anisotropy in this plane was substantially greater in the oxidized structures.

Because of the obvious positional disorder of the A-site cations, a variety of split-atom models using only Na, as well as both Na and K, was tested using combinations of A(2), A(*m*), and A(2/*m*) (see Hawthorne, 1983, p. 254–257). For each model, the unconstrained occupancies, isotropic temperature factors, and appropriate coordinates were refined simultaneously for the split atoms as part of a full-matrix refinement with parameter shifts dampened to 0.5. Two criteria were used to test the models: (1) reasonable values of *B* should obtain for all sites; (2) a given model should perform satisfactorily for all three structures.

The model that best fit these criteria involved only Na and only A(2) and A(*m*). However, difference-Fourier syntheses indicated small residuals at A(2/*m*) for the natural (H-1) and hydrothermally treated (H-11) structures, but not for the air-heated structure (H-3). The data for this model (Table 9) should be viewed with caution. It is quite likely that these split-atom positions themselves represent considerable averaging. Furthermore, on the basis of energy calculations and probability studies, Docka et al. (1987) have concluded that the general position, A(1), is usually the most probable site for A-cation occupancy although there is a significant probability for occupancy at A(2), A(*m*), and A(2/*m*) as well.

The M(4′) site. It has been found that in calcic and sodic-calcic amphiboles, small amounts of Fe (or Mn) present at M(4) tend to order at a distinct M(4′) site rather than at the principal M(4) site occupied by Ca and Na (Bocchio et al., 1978; Ungaretti et al., 1981). By locating in this position, the Fe (or Mn) achieves a coordination environment similar to the M(4) site in grunerite (Ungaretti et al., 1981).

TABLE 9. Positional parameters, B_{iso}, occupanices (electrons per site), and interatomic distances (Å) for A(*m*) and A(2)

		x	*y*	*z*	B_{iso}	Electrons per site
A(*m*)	H-1	0.017(2)	0.5	0.044(3)	1.3(2)	1.08(4)
	H-11	0.046(2)	0.5	0.094(3)	1.6(2)	1.05(5)
	H-3	0.055(3)	0.5	0.113(5)	3.5(4)	1.77(10)
A(2)	H-1	0.0	0.472(1)	0.0	2.1(3)	1.15(5)
	H-11	0.0	0.485(1)	0.0	2.2(2)	1.30(5)
	H-3	0.0	0.486(1)	0.0	2.1(4)	1.11(7)

	H-1	H-11	H-3
A(*m*)–O(5) ×2	3.04(1)	3.02(1)	3.02(1)
–O(5) ×2	3.07(1)	3.18(1)	3.21(1)
–O(6) ×2	2.97(1)	2.75(1)	2.67(1)
–O(6) ×2	3.33(1)	3.57(2)	3.65(2)
–O(7)	2.47(2)	2.53(2)	2.53(2)
–O(7)	2.56(2)	2.58(2)	2.61(2)
–O(7)	3.49(1)	3.20(2)	3.08(2)
–O(7)	3.97(2)	4.25(2)	4.35(3)
–O(3)	3.55(2)	3.26(2)	3.18(2)
–O(3)	3.92(2)	4.22(2)	4.32(2)
A(2)–O(5) ×2	2.64(2)	2.82(1)	2.83(1)
–O(5) ×2	3.48(3)	3.28(1)	3.25(2)
–O(6) ×2	2.82(2)	2.95(1)	2.95(1)
–O(6) ×2	3.51(2)	3.33(1)	3.30(1)
–O(7) ×2	2.557(6)	2.505(3)	2.487(4)
–O(7) ×2	3.763(5)	3.727(2)	3.712(3)
–O(3) ×2	3.765(5)	3.739(2)	3.737(3)
A(2)–A(*m*)	0.57(2)	0.64(2)	0.74(2)

Note: Estimated standard deviations are given in parentheses and refer to the least significant digit.

For all three structures, difference-Fourier syntheses indicated small residuals at 0,0.2500,0.5 corresponding to the M(4′) sites. Various attempts to refine M(4′) proved less than satisfactory because of the close proximity to M(4) and the high correlations among M(4) and M(4′) parameters. Ultimately, the occupancies of the M(4′) sites were refined using scattering factors for Fe with other parameters fixed at $y = 0.2500$ and $B = 0.80$. These refinements yielded M(4′) site occupancies of 0.011(1), 0.007(1), and 0.009(2) Fe for H-1, H-11, and H-3, respectively. It is quite possible that these values represent Mn, which was found in minor amounts by microprobe analysis, rather than Fe.

Infrared data

Figure 3 shows the infrared spectra of H-1, H-11, and H-3 between 3750 and 3550 cm^{-1}. This region has been associated with the fundamental hydroxyl stretch frequencies in amphiboles (see Hawthorne, 1981b, 1983). The intensity of the O–H bond will be dependent upon both the number and type of metal cations coordinated to the hydroxyl group. In the amphibole structure, each hydroxyl group is coordinated by one M(3) and two M(1) cations in a pseudotrigonal arrangement. For amphiboles with only two types of metal ions, e.g., Fe^{2+} and Mg^{2+}, there will be four distinguishable combinations. However, for each additional cation type present, the number

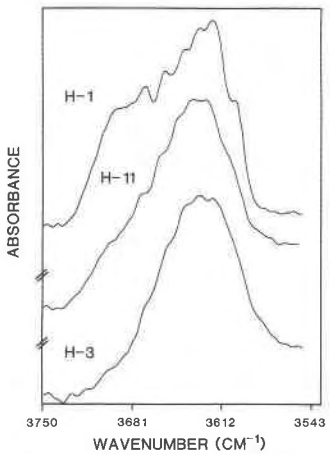

Fig. 3. The infrared absorption spectra for H-1, H-11, and H-3.

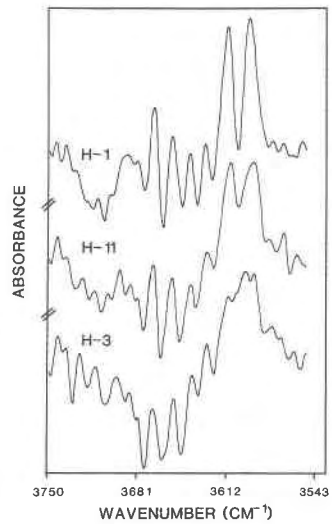

Fig. 4. The first-derivative spectra for H-1, H-11, and H-3 derived from the infrared absorption spectra shown in Fig. 3.

of possible combinations is increased by $3(n-1)$, where n is the total number of cation types. Hence, in a hornblende that can contain 4 or 5 different octahedral cations at M(1) and M(3), there will be 19 or 31 different combinations, respectively. Relatively minor frequency shifts may be induced depending on the type of cations at M(4) and M(2) (see Hawthorne, 1983); however, occupancy of the A site leads to dramatic shifts toward higher frequencies. Displacements ranging from $+24$ cm^{-1} in riebeckite (Strens, 1974) up to $+62$ cm^{-1} in a potassian richterite (Rowbotham and Farmer, 1973) have been reported. In H-1, H-11, and H-3, roughly half of the A sites are occupied; therefore, the spectra shown in Figure 3 include stretch frequencies for O–H groups adjacent to vacant A sites as well as those shifted to higher frequencies because of A-cation perturbations.

The infrared spectrum of natural hornblende was previously described as a broad and jagged band (Burns and Strens, 1966). However, because of the Fermat advantage, the multiple scans collected using a Fourier-transform technique greatly enhance the signal-to-noise ratio as shown in Figure 3. Therefore, it was possible to resolve at least some of the features of these spectra, although it was not possible to measure the intensities of the fundamental hydroxyl stretch frequencies with sufficient accuracy for meaningful determination of cation site occupancies. The peak positions given in Table 10 were determined using first-derivative spectral analysis (Fig. 4) of the previously measured spectra (Fig. 3).

The $Fe^{2+}Fe^{2+}Fe^{2+}$ combination in other amphiboles has been previously assigned to peaks ranging between 3624 and 3617 cm^{-1} (Burns and Strens, 1966). It seems likely that the peak observed at 3621 cm^{-1} for these samples is also due to the $Fe^{2+}Fe^{2+}Fe^{2+}$ cation combination. Starting with this assumption, peak displacements relative to the 3621-cm^{-1} frequency were used to identify additional peaks. The assignments given in Table 10 are based on previous investigations performed on a variety of amphiboles by Bancroft and Burns (1969), Burns and Prentice (1968), Burns and Strens (1966), Ernst and Wai (1970), and Strens (1974).

When H is lost from an O(3) oxygen as part of the oxidation-dehydrogenation process, it no longer contributes to the hydroxyl stretch frequency, and information regarding the coordination environment of that O(3) is lost. Therefore, interpretation of the changes in the M-site cation distributions in these structures is not warranted because of the appreciable increase in oxy-amphibole content from H-1 to H-11 to H-3.

The most notable feature in these spectra (Fig. 3) is the decrease in overall band width from H-1 to H-11 to H-3, respectively. This decrease is primarily due to signal attenuation in the high-frequency region associated with A-site cation perturbations. This attenuation with progressive oxidation indicates that dehydrogenation preferentially occurs at O(3) sites adjacent to A sites that are occupied rather than vacant.

Discussion

Phillips et al. (1988a, 1988b) have recently proposed a preliminary model to explain the oxidation behavior of Fe in amphiboles. The basic tenets of this model are (1) as oxidation by dehydrogenation occurs, a local charge imbalance is created at the O(3) site; (2) in order to offset this imbalance, a number of compensation mechanisms are initiated; (3) oxidation by dehydrogenation proceeds only to the extent that these compensation mechanisms can adequately maintain structural stability (or at least metastability) as gauged by bond strengths; and (4) beyond this point, the structure "exsolves" iron oxide, which actually represents the initial stages of decomposition.

Although there is no evidence for partial decomposition in these structures, the compensation mechanisms described by Phillips et al. (1988a) were activated by ox-

Table 10. Band positions and tentative configuration assignments

Peak positions (cm^{-1})			
H-1	H-11	H-3	Configuration
—	3695	3697	These bands represent configurations that are perturbed by A-site cations
3691	—	—	
3687	3686	3686	
3682	3680	3680	
3672	3670	3670	MgMgMg
3657	3653	3653	$MgMgFe^{+2}$ or MgMgAl
3641	3639	3639	$MgFe^{2+}Fe^{2+}$
3630	3630	3631	$MgFe^{2+}Fe^{3+}$*
3621	3621	3621	$Fe^{2+}Fe^{2+}Fe^{2+}$
—	—	3618	$Fe^{2+}Fe^{2+}Fe^{3+}$
—	—	3608	$Fe^{2+}Fe^{3+}Fe^{3+}$
3604	3605	3604	$Fe^{3+}Fe^{3+}Fe^{3+}$

* $MgFe^{3+}Fe^{3+}$, $Fe^{2+}AlAl$, and $Fe^{2+}Fe^{2+}Al$ are also possibilities.

idation in H-11 and H-3. There is compensational shortening of the individual M–O(3) bond lengths as evidenced by comparison of M(1)–O(3) to M(1)–O(1) in the three structures (Table 4). Furthermore, as oxidation-dehydrogenation progressed, there was preferential ordering of Fe^{3+} (and perhaps Al) at M(1) and M(3) as indicated by the increases in the parameter $\Delta\langle M\text{–}O\rangle$ (Figs. 1A and 1C). The increased trivalent contents of the M(1) and M(3) sites in H-11 and H-3 represent not only Fe^{3+} produced by oxidation, but also trivalent cations originally residing at M(2) as evidenced by the decrease in $\Delta\langle M\text{–}O\rangle$ with increasing oxidation (see Fig. 1B). In addition, there are several indications that with dehydrogenation at O(3), there is interaction between some A-site cations and O(3). The A(m)–O(3) distance progressively decreased with increasing dehydrogenation, and the occupancy of A(m) increased in H-3, apparently at the expense of M(4) and A($2/m$) (see Table 9). In a compositionally similar hornblende heated in air for 20 h, Ungaretti (personal communication, 1987) has found an even shorter A(m)–O(3) distance. The decrease in the band width of the infrared spectra (Fig. 3) with increasing oxidation-dehydrogenation suggests that dehydrogenation preferentially occurs at O(3) sites in the vicinity of an occupied, rather than a vacant, A site. This behavior would also be expected if the A cation plays a role in partially compensating the loss of bond strength at O(3) that results from dehydrogenation.

Acknowledgments

The original manuscript was improved by comments and suggestions from Maryellen Cameron and, in particular, Roger Burns. Useful suggestions regarding aspects of the refinement procedures were made by Luciano Ungaretti. The manuscript was typed by Karen Bird. The X-Ray Diffraction Facility at the University of Toledo is maintained and operated through support from the College of Arts and Sciences. This work was also supported by NSF Grants EAR-8312878 and EAR-8816257 to R.K.P. and EAR-8816650 to M.W.P.

References cited

Bancroft, G.M., and Burns, R.G. (1969) Mössbauer and absorption spectral studies of alkali amphiboles. Mineralogical Society of America Special Paper 2, 137–148.

Barnes, V.E. (1930) Changes in hornblende at about 800 °C. American Mineralogist, 15, 393–417.

Bocchio, R., Ungaretti, L., and Rossi, G. (1978) Crystal-chemical study of eclogitic amphiboles from Alpe Arami, Lepontine Alps, southern Switzerland. Rendiconti della Società Italiana di Mineralogia e Petrologia, 34, 453–470.

Brown, I.D., and Wu, K.K. (1976) Empirical parameters for calculating cation-oxygen bond valences. Acta Crystallographica, B32, 1957–1959.

Burns, R.G., and Prentice, F.J. (1968) Distribution of iron cations in the crocidolite structure. American Mineralogist, 53, 770–776.

Burns, R.G., and Strens, R.G.J. (1966) Infrared study of the hydroxyl bands in clinoamphiboles. Science, 153, 890–892.

Clowe, C.A., Popp, R.K., and Fritz, S.J. (1988) Experimental investigation of the effect of oxygen fugacity on ferric-ferrous ratios and unit-cell parameters of four natural clinoamphiboles. American Mineralogist, 73, 487–499.

Cruickshank, D.W.J. (1965) Errors in least-squares methods. In J.S. Rollett, Ed., Computing methods in crystallography, p. 112–116. Pergamon Press, New York.

Docka, J.A., Post, J.E., Bish, D.L., and Burnham, C.W. (1987) Positional disorder of A-site cations in $C2/m$ amphiboles: Model energy calculations and probability studies. American Mineralogist, 72, 949–958.

Ernst, W.G., and Wai, C.M. (1970) Mössbauer, infrared, X-ray, and optical study of cation ordering and dehydrogenation in natural and heat-treated sodic amphiboles. American Mineralogist, 55, 1226–1258.

Fritz, S.J., and Popp, R.K. (1985) A single-dissolution technique for determining FeO and Fe_2O_3 in rock and mineral samples. American Mineralogist, 70, 961–968.

Hawthorne, F.C. (1981a) Crystal chemistry of the amphiboles. Mineralogical Society of America Reviews in Mineralogy, 9A, 1–102.

——— (1981b) Amphibole spectroscopy. Mineralogical Society of America Reviews in Mineralogy, 9A, 103–139.

——— (1983) The crystal chemistry of the amphiboles. Canadian Mineralogist, 21, 173–480.

Hawthorne, F.C., and Grundy, H.D. (1977) The crystal chemistry of the amphiboles: III. Refinement of the crystal structure of a sub-silicic hastingsite. Mineralogical Magazine, 41, 43–50.

Ibers, J.A., and Hamilton, W.C. (1964) Dispersion corrections and crystal structure refinements. Acta Crystallographica, 17, 781–782.

International tables for X-ray crystallography. (1974) Volume IV, Tables 2.2B and 2.3.1. Kynoch Press, Birmingham, England.

North, A.C.T., Phillips, D.C., and Mathews, F.S. (1968) A semi-empirical method of absorption correction. Acta Crystallographica, A24, 351–359.

Papike, J.J., Ross, M., and Clark, J.R. (1969) Crystal-chemical characterization of clinoamphiboles based on five new structure refinements. Mineralogical Society of America Special Paper 2, 117–136.

Phillips, M.W., Popp, R.K., and Clowe, C.A. (1988a) Structural adjustments accompanying oxidation-dehydrogenation in amphiboles. American Mineralogist, 73, 500–506.

Phillips, M.W., Popp, R.K., Clowe, C.A., and Pinkerton, A.A. (1988b) Oxidation-induced "exsolution" of iron oxide in grunerite (abs.). EOS, 69, 523.

Rowbotham, G., and Farmer, V.C. (1973) The effect of "A" site occupancy on the hydroxyl stretching frequency in clinoamphiboles. Contributions to Mineralogy and Petrology, 38, 147–149.

Spear, F.S. (1982) Phase equilibria of amphibolites from the Post Pond volcanics, Mt. Cube quadrangle, Vermont. Journal of Petrology, 23, 383–426.

Strens, R.G.J. (1974) The common chain, ribbon, and ring silicates. In V.C. Farmer, Ed., The infrared spectra of minerals. Mineralogical Society, London.

Ungaretti, L. (1980) Recent developments in X-ray single crystal diffrac-

tometry applied to the crystal-chemical study of amphiboles. Godisnjak Jugoslavenskog Centra za Kristalografiju, 15, 29–65.

Ungaretti, L., Smith, D.C., and Rossi, G. (1981) Crystal-chemistry by X-ray structure refinement and electron microprobe analysis of a series of sodic-calcic to alkali-amphiboles from the Nybö eclogite pod, Norway. Bulletin de Minéralogie, 104, 400–412.

Walker, N., and Stuart, D. (1983) An empirical method for correcting diffractometer data for absorption effects. Acta Crystallographica, A39, 158–166.

Zachariasen, W.H. (1963) The secondary extinction correction. Acta Crystallographica, 16, 1139–1144.

——— (1967) A general theory of X-ray diffraction in crystals. Acta Crystallographica, 23, 558–564.

Manuscript received June 3, 1988
Manuscript accepted March 6, 1989